# Noise properties of low-dose X-ray CT sinogram data in Radon space

Jing Wang[1], Hongbing Lu[2], Zhengrong Liang[1], Daria Eremina[3], Guangxiang Zhang[4], Su Wang[1], John Chen[4], and James Manzione[1]

Departments of Radiology[1], Applied Mathematics & Statistics[3], and Preventive Medicine[4], State University of New York, Stony Brook, NY 11794, USA
Department of Biomedical Engineering/Computer Application[2], Fourth Military Medical University, Xi'an, Shaanxi 710032, China

## ABSTRACT

Computed tomography (CT) has been well established as a diagnostic tool through hardware optimization and sophisticated data calibration. For screening purposes, the associated X-ray exposure risk must be minimized. An effective way to minimize the risk is to deliver fewer X-rays to the subject or lower the mAs parameter in data acquisition. This will increase the data noise. This work aims to study the noise property of the calibrated or preprocessed sinogram data in Radon space as the mAs level decreases. An anthropomorphic torso phantom was scanned repeatedly by a commercial CT imager at five different mAs levels from 100 down to 17 (the lowest value provided by the scanner). The preprocessed sinogram datasets were extracted from the CT scanner to a laboratory computer for noise analysis. The repeated measurements at each mAs level were used to test the normality of the repeatedly measured samples for each data channel using the Shapiro-Wilk statistical test merit. We further studied the probability distribution of the repeated measures. Most importantly, we validated a theoretical relationship between the sample mean and variance at each channel. It is our intention that the statistical test and particularly the relationship between the first and second statistical moments will improve low-dose CT image reconstruction for screening applications.

**Keywords:** Low-dose CT, screening application, sinogram data, statistical moments, noise reduction.

## 1. INTRODUCTION

Computed tomography (CT), performing image reconstruction from Radon space measurement, has been well established as a diagnostic modality through hardware optimization and sophisticated data calibration [1, 6]. However, clinical use of CT frequently exposes the patients to excessive X-ray radiation [4]. For screening and image-guided interventional purposes, the associated X-ray exposure risk to the subjects and operators should be minimized. An effective way to minimize the risk is to deliver less X-rays to the subject or decrease the mAs value in the data acquisition protocol to a level as low as achievable for a concerned clinical task. As the mAs value decreases, the noise level of the calibrated data increases and is the underlying fundamental problem.

The noise is introduced during X-ray generation from the X-ray source and then propagates along as X-rays traverse the body and pass through the detection system [6]. The detected counts reflect the transmitted X-ray photon numbers and their energies. Studying the noise properties of the transmitted data is currently an attractive research topic [10]. To reconstruct an acceptable quality image, the transmitted data must be calibrated. While most of the calibration operations are system specific, a mathematical logarithm transform which converts the transmitted data into Radon space is common to all CT systems [6, 10]. Hereafter, the system calibrated and logarithm transformed data is referred to as the preprocessed sinogram or simply sinogram. This work aims to study the noise property of the sinogram as the mAs level decreases. It is expected that the acquired knowledge on the noise properties could improve the well-established Radon-space CT image reconstruction methodologies [1] and lead to minimized X-ray exposure risk in clinical applications.

[1] Corresponding author: Z. Liang, Email: jzl@mil.sunysb.edu; Phone: (631) 444-7837; Fax: (631) 444-6450.

Medical Imaging 2008: Physics of Medical Imaging, edited by Jiang Hsieh, Ehsan Samei,
Proc. of SPIE Vol. 6913, 69131M, (2008) · 1605-7422/08/$18 · doi: 10.1117/12.771153

## 2. THEORY

While the noise propagation through detection and calibration operations is a very complicated process, the noise distribution at the X-ray generation stage can be expressed as a Poisson functional [6]. Consider the polyenergetic nature of X-ray generation where the Poisson function becomes a compound Poisson form which includes a convolution with the X-ray energy spectrum [7, 10]. The convolution operation may alter the Poisson distribution [7]. Additional calibration operations including the logarithm transform can further alter the Poisson distribution [5, 10]. The data mean remains unaltered, however, the variance changes noticeably as the noise propagates through these calibration operations [2, 5, 10]. In the following, we will focus on the mean-variance relationship of the Poisson distribution in Radon space and present a modified mean-variance functional formula which accommodates the variance variation due to the preprocessing calibration operations and other factors, such as inclusion of background noise. A major reason for focusing on the mean-variance relationship is because these first and second statistical moments play an essential role in noise treatment for low-dose CT applications.

### 2.1 Statistical Distributions of Emitted and Transmitted X-ray Photons

The emission of photons from the X-ray source is a Poisson process with probability given by [6]

$$P_k(N_0) = \frac{N_0^k e^{-N_0}}{k!} \tag{1}$$

where $P_k$ is the probability, in a given time interval, of emitting *k* photons, and $N_0$ is the average number of photons emitted during that interval. The process of photon transmission through the body is described by a binary process where photons are either removed or transmitted. This process can be described by a binomial model in which the probability *prob* of a photon being transmitted is $\exp(-\int_{-\infty}^{+\infty} \mu \, ds)$ and the probability of a photon being removed is 1-*prob*, where $\mu$ represents the linear attenuation coefficient and *ds* indicates a length element along the photon path [6]. It has been shown that the cascading of the Poisson and binomial distributions results in a Poisson distribution [6], i.e., the exit or transmitted photons from the body continue to be Poisson distributed with the rate scaled by the transmission probability $prob = \exp(-\int_{-\infty}^{+\infty} \mu \, ds)$. Hereafter $p = \int_{-\infty}^{+\infty} \mu \, ds$ is called line integral of the attenuation coefficients.

### 2.2 Mean and Variance of the Line Integral

It has been shown that the mean of the transmitted photon number is a nonlinear function of the line integral of the attenuation coefficient, i.e., $N_d = N_0 \exp(-\int \mu \, \mathrm{d}s)$ [6]. Ideally, the line integral at the detector bin or data channel *i* can be calculated by

$$p_i = \ln \frac{N_0}{\kappa} = \ln N_0 - \ln \kappa \tag{2}$$

where $\kappa$ is a random variable representing the number of transmitted photons at that channel and it follows a Poisson distribution with the mean value $N_d$. Therefore the measured line integral $p_i$ will also be a random variable. By the use of the Taylor expansion, it has been shown in [6] that the mean $\bar{p}_i$ and variance $\sigma_{p_i}^2$ of $p_i$ are given respectively by

$$\bar{p}_i = \ln(N_0 / N_d) \quad \text{and} \quad \sigma_{p_i}^2 = 1/N_d \,. \tag{3}$$

Therefore the relationship between the mean and variance of the line integral can be described by the following formula

$$\sigma_{p_i}^2 = \frac{1}{N_0} \exp(\bar{p}_i) \tag{4}$$

To accommodate deviation from the Poisson distribution due to the polyenergetic nature of X-ray generation and the necessary data calibration operations, the mean-variance relationship (4) could be replaced by [2]

$$\sigma_{p_i}^2 = f_i \exp(\overline{p}_i / \eta) \quad (5)$$

where $\eta$ is a scaling parameter which enables the measured photon energies to be stored as integers while retaining the dynamic range of the line integrals of the attenuation coefficients. It is system specific, and different CT manufacturers may choose different $\eta$ values. Notation $f_i$ in equation (5) represents an adjustable factor adaptive to each detector bin *i*. It mainly considers different incident photon numbers at different detector bins. The magnitude of $f_i$ is primarily determined by the mAs level (which reflects the output photon flux density from the X-ray source). At a specific mAs level, the values of $f_i$ at different detector bins are mainly affected by the Bowtie attenuating filtration across the field of view (FOV) [6]. Some small variation among neighboring $f_i$ values may reflect the bin-by-bin calibration operations on the uniformity of X-ray generation and detector-bin response. It is also system specific, and its dependence on index *i* is mainly due to the Bowtie filter and bin-by-bin calibration. The parameters $\eta$ and $f_i$ are object-independent because their theoretical basis is equation (4), which is derived without any assumption about the object. Their values can be completely determined given the CT system settings. In the following, we will study the noise properties of the sinogram by repeated scans of an anthropomorphic torso phantom with the focus on the validation of the mean-variance relationship (5).

## 3. EXPERIMENTAL PHANTOM RESULTS

Repeated phantom experiments were performed using a Siemens SOMATOM Sensation16 CT scanner and an anthropomorphic torso phantom of Figure 1 (Radiology Support Devices, Inc., Long Beach, CA). The data acquisition protocol included a tube voltage of 120 kVp, 1.5 mm slice thickness and rotation speed of 0.5 seconds per rotation. A total of five different mAs levels were chosen from 100 down to 17 (the lowest provided by the CT scanner): 100, 80, 60, 40, and 17 mAs. At each mAs level, the CT scanner revolved 150 times around the phantom. Each rotation included 1160 projection views evenly spaced on a circular orbit. Each view included 672 detector bins. The detector arrays were on an arc concentric to the X-ray source with a distance of 1040 mm. The distance from the rotation center to the X-ray source was 570 mm. The detector bin spacing was 1.407 mm. The scaling parameter $\eta$ is 2294.5 for the Siemens CT system.

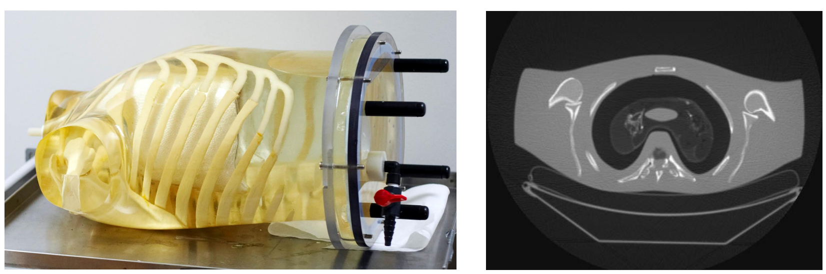

Figure 1: Illustration of the anthropomorphic torso phantom (left) and a CT image of the transverse cross section of the thorax phantom (right).

From the 150 repeated scans at each mAs level, we calculated the sample mean $\overline{p}_i$ and variance $\sigma_{p_i}^2$ for each channel. There were a total of 672×1160 channels. Given the calculated pair $\{\overline{p}_i, \sigma_{p_i}^2\}$ and the scaling parameter $\eta$, the value of $f_i$ was computed according to equation (5). At each projection view, we plotted a curve of $\{f_i\}$ across the 672 detector bins. The curves from all 1160 views were essentially the same. Figure 2 shows the curves $\{f_i\}$ averaged over the 1160 projection views at the five different mAs levels. It can be observed that the shapes of the curves are similar. The shape is also similar to the result in the absence of an object in the FOV as shown in [10], where the curve shape is mainly caused by the Bowtie filter used for attenuating the incident X-ray beams across the FOV. It can also be observed that small spikes are present along the curve of $f_i$ regularly spaced across the FOV. This phenomenon may be caused by the transition between detector modules.

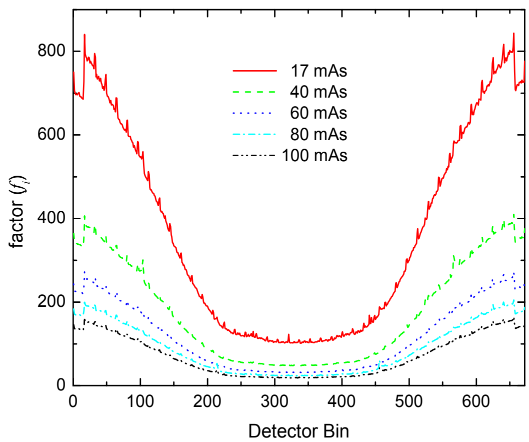


Figure 2: The factor $f_i$ in equation (5) calculated from repeated measurements at different mAs levels. Each curve represents an average over the 1160 views.

The similarity of { $f_i$ } curves for different mAs levels was further studied by plotting the paired points ( $f_{i,100}$ , $f_{i,mAs}$ ), where $f_{i,100}$ is the $f_i$ value at the 100 mAs level while $f_{i,mAs}$ is the value at a lower mAs level. Figure 3 shows the plots of the paired points. A linear relationship can be observed for each of the four mAs levels. The slopes of these four lines were determined by linear fitting and their values are shown by the four points at 17, 40, 60, 80 mAs in Figure 4. Essentially, all these four slope values are closely represented by the corresponding ratios of $f_{i,mAs} / f_{i,100}$ . The relationship between the ratios of $f_{i,mAs} / f_{i,100}$ and the mAs levels can be described by a reciprocal function:

$$y = 1/(a + bx) \tag{6}$$

as shown in Figure 4. Ideally, the ratios of $f_{i,mAs} / f_{i,100}$ would be inversely proportional to the number of incident photons or mAs level, i.e., the parameter $a$ in equation (6) would be zero. However, at low mAs levels, the electronic background noise will have a noticeable contribution to the total noise level. The background noise is considered by $f_i$ in equation (5) via the parameter $a$.

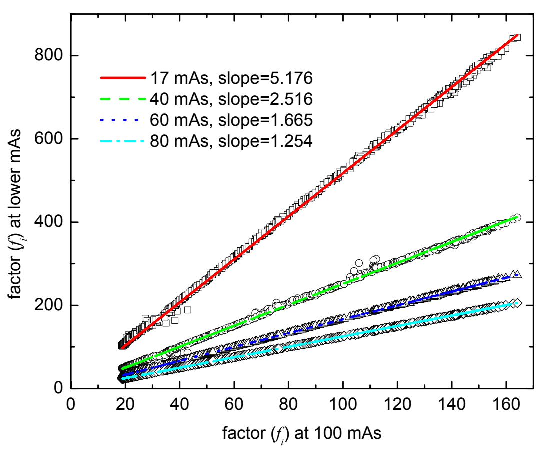


Figure 3: Illustration of the linear relationship between the $f_i$ value at the 100 mAs level.

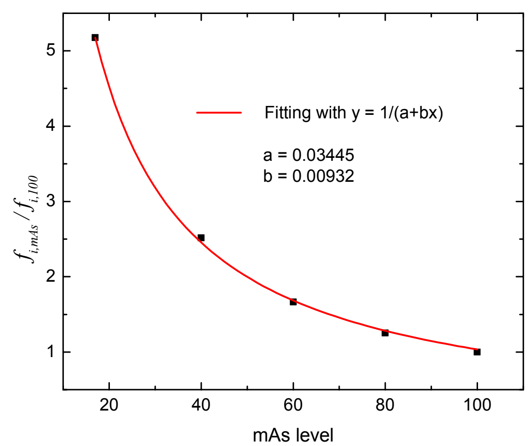


Figure 4: The factors of $f_{i,mAs} / f_{i,100}$ at the five mAs levels and their fitted curve with a reciprocal functional. Given this curve and the shape of $f_i$ in Figure 2, the variance at any mAs level can be estimated.

The similarity of { $f_i$ } curves for different attenuating conditions (i.e., 1160 view angles around the anthropomorphic torso phantom) and different mAs levels for each view angle indicates that parameter $f_i$ is object-independent, concurring with the theoretical analysis in Section II. Its global shape reflects the Bowtie filtration and its local variation indicates the detector bin response. Given the shape of $\{f_i\}$ in Figure 2 and the curve of $f_{i,mAs} / f_{i,100}$ in Figure 4, we are able to estimate the variance of the sinogram at any mAs level by the theoretical model (5) for practical purposes.

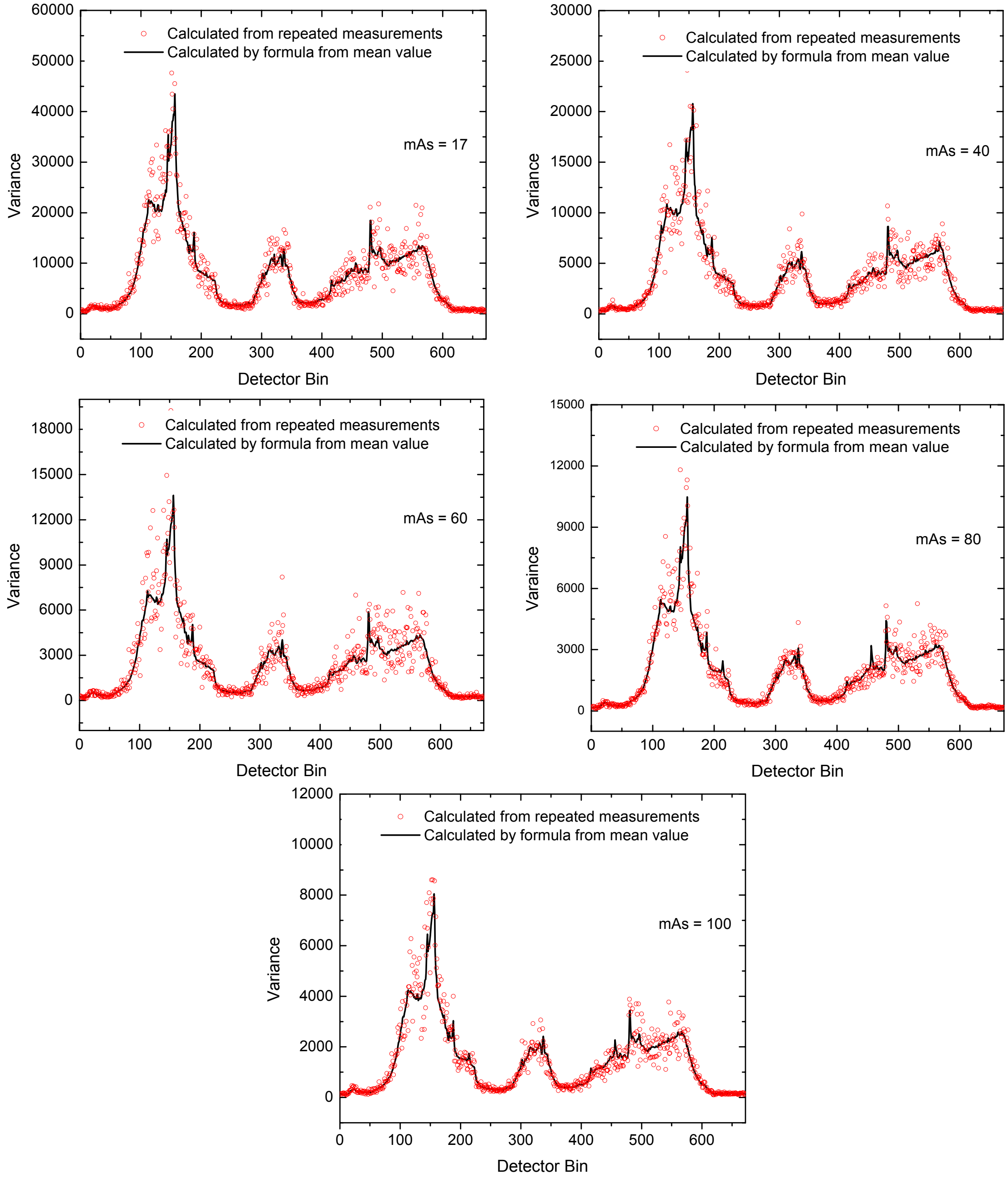


Figure 5: Illustration of the sinogram data variances calculated from repeated scans and from equation (5). (top left) – result at 17 mAs, (top right) – result at 40 mAs, (middle left) – result at 60 mAs, (middle right) – result at 80 mAs, and (bottom) – result at 100 mAs. These variances from repeated scans and from prediction of equation (5) agree with each other very well.

To further validate the above noise model (5) across the FOV, we compared the experimental sample variances calculated from the repeated scans with the theoretical variances predicted by equation (5) for each of the 1160 views. An example is presented below for an arbitrarily selected projection view. For each mAs level, the experimental sample variances for that view have been calculated previously when we computed the pairs ( $\overline{p}_i$ , $\sigma^2_{p_i}$ ) for each detector bin $i$ for a total of 672 bins. The theoretical variances were determined as follows. Given the sample mean $\overline{p}_i$ at that view and the above determined parameter $f_i$ from all 1160 views and $\eta$ =2294.5 for the CT system, the corresponding theoretical variance $\sigma^2_{p_i}$ can be computed by (5). Figure 5 compares the experimental sample variances and the theoretically predicted variances for each mAs level at the selected view, where a good consistency is observed for all mAs levels. To quantitatively measure the consistency between the variance predicted by (5) and the experimental sample variance calculated from the repeated scans, we computed the Lin's concordance correlation coefficients [3] at all mAs levels. The results are shown in Table I. It can be observed that all of Lin's concordance coefficients are larger than 0.9, even in the cases where all lower bounds of the 95% confidence interval of the correlation coefficients are larger than 0.9, suggesting an excellent agreement between experimental and predicted variances. This agreement was also visually seen from repeated measurements of a different CT scanner (a GE HiSpeed four-slice CT scanner) as reported in [2].

Table I: Lin's concordance correlation coefficient between experimental and theoretical variances at different mAs levels.

| mAs level | Sample Size N | Lin's Concordance Coefficient | 95% Confidence Interval of Concordance Coefficient |
|---|---|---|---|
| 100 | 672 | 0.958 | (0.952, 0.964) |
| 80 | 672 | 0.961 | (0.954, 0.966) |
| 60 | 672 | 0.913 | (0.900, 0.925) |
| 40 | 672 | 0.941 | (0.932, 0.949) |
| 17 | 672 | 0.953 | (0.945, 0.959) |

In the following, we turn our attention to the normality test of the repeatedly measured samples for each channel. The statistical normality test was performed for all detector bins (i.e., 672) over all projection views (i.e., 1160), or a total of 672×1160 channels with each channel consisting of 150 random samples. The Shapiro-Wilk normality test was employed via the use of the program *R*, which is a free software environment for statistical analysis and can be downloaded at (http://www.r-project.org/index.html).

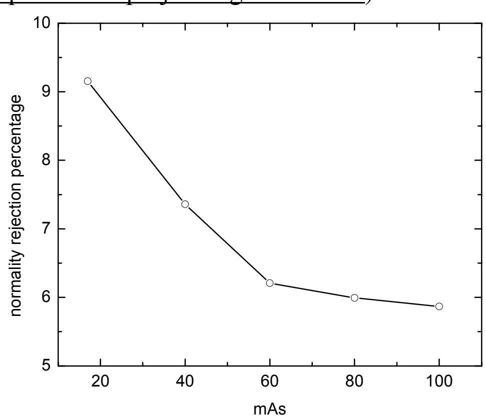


Figure 6: Rejection percentage of the Shapiro-Wilk normality test for the sinogram data at different mAs levels.

The null hypothesis $H_0$ in the normality test is stated as follows. The acquired 150 data values from each channel are random samples from a normal distribution. If the probability (p-value) is less than the level of significance (e.g., 0.05 for 95% level was chosen in this study), then the null hypothesis is rejected. The Shapiro-Wilk test gives the p-value for each of the 150 repeated measurements at each channel. A smaller p-value indicates that the projection data at that channel is less likely to follow a normal distribution. The rejection percentage (those channels whose p-values are less than 0.05 divided by the total number of channels in each sinogram) for each mAs level is shown in Figure 6. It can be observed that the rejection percentages increased from approximately 6% at 100 mAs level up to 9% at 17 mAs level for all data channels.

To view the p-value distribution across the FOV, we plotted Figure 7, which shows the relationship between projection mean value and Shapiro-Wilk test p-value at different detector bins at a projection view. Figure 7(left) shows the result from the 17 mAs level and Figure 7(right) represents the result from the 100 mAs level. Compare the Shapiro-Wilk test p-values at the 17 mAs level with that at the 100 mAs level for the same projection view, we can observe that small p-values less than 0.05 occur mostly at those detector bins where the X-rays pass through the most dense parts of the body, corresponding to the high projection mean values or low-flux transmitted data. As the mAs level decreases, less X-ray photons will be generated and detected and, therefore, less projection data will pass the Shapiro-Wilk normality test.

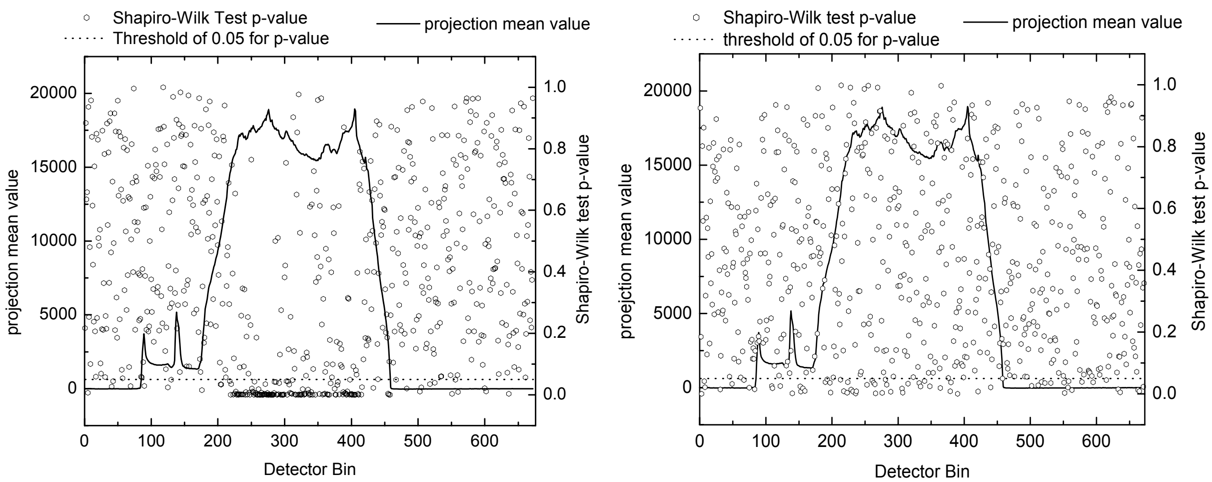


Figure 7: Relationship between the projection mean value and the Shapiro-Wilk test p-value at different detector bins by the same projection view for the 17 mAs (left) and the 100 mAs (right) levels.

Based on Figure 7, we further computed the rejection percentage at the low flux region. For those high projection-mean values greater than 10000, the rejection percentage increased from 7.03% at 100 mAs level to 18.40% at 17 mAs level. The rejection percentage increased at a higher speed for a larger projection-mean value. For example, the rejection percentage increased from 9.95% at 100 mAs level to 41.95% at 17 mAs for projection mean values greater than 15000.

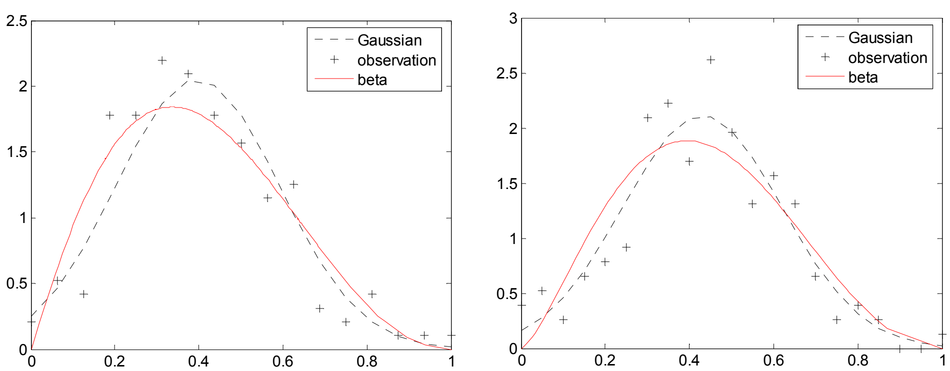


Figure 8: Probability density function from detector bin #120 (left) and #376 (right) at the 17 mAs level. Its corresponding p-value from the Shapiro-Wilk test is 0.001. The dotted line represents a fitting to a Gaussian distribution. The solid line shows a fitting to a Beta function.

For those detector bins with p-values less than 0.05 at the 17 mAs level in Figure 7, we further studied their noise distribution in terms of probability density function (PDF). Figure 8 shows, as an example, the PDF from detector bin #120 (left) and detector bin #376 (right) at the 17 mAs level in Figure 7. Their corresponding p-values from the Shapiro-Wilk normality test is 0.001. It can be observed that for a very small p-value (i.e., a highly likely non-normal distribution), the PDF did reveal some deviation from a Gaussian distribution. The deviation from a normal distribution can be quantitatively measured by higher statistical moments, such as skewness and kurtosis. Table II lists the statistical moments for several detector bins with high mean values at the 17 mAs level and small p-values (<0.05) from the Shapiro-Wilk normality test. It can be observed that for those detector bins with small p-value (<0.05) from the Shapiro-Wilk normality test, their corresponding skewness or kurtosis are generally non-zero (both skewness and kurtosis would be zero for Gaussian distribution). It is noted that despite the deviation from a normal distribution as seen in Figure 8, the measured PDF fits Gaussian better than Poisson, Gamma and Beta functional forms because all of these latter distributions do not have the mean-variance relationship of (5) [5]. The fitting to the Beta distribution is shown in Figure 8 as an example. Both the Gamma and Beta functions are much more complicated in numerical calculation than the Poisson and Gaussian forms.

Table II: Statistics for the detector bins with high mean value.

| Detector Bin | Mean Value | Normality Test p-value | Skewness | Kurtosis |
|---|---|---|---|---|
| 376 | 16118 | 0.00103 | -0.09708 | -0.67877 |
| 377 | 15994 | 7.890E-7 | 0.32897 | 0.73426 |
| 378 | 15918 | 0.17249 | 0.20178 | 0.48699 |
| 379 | 16027 | 0.03228 | -0.16628 | 0.11167 |
| 380 | 16171 | 0.04202 | 0.12740 | -0.28743 |
| 381 | 16281 | 0.61378 | 0.13290 | -0.00143 |
| 382 | 16428 | 0.00134 | 0.11541 | 0.29458 |
| 383 | 16595 | 0.16667 | 0.23176 | 0.02940 |
| 384 | 16758 | 0.09693 | -0.03816 | -0.05951 |
| 385 | 16837 | 0.14875 | 0.17857 | -0.14606 |

In addition to the studies on the mean-variance relationship and the normality tests of noise distribution in the sinogram, we also analyzed the noise correlation among different bins. Figure 9(left) displays the correlation coefficients matrix of the noise among detector bins at one view from the repeated measurements of the Siemens scanner at the 17 mAs level. Figure 9(right) shows the horizontal profiles through the center of Figure 9(left). The average of the off-diagonal values from Figure 9(left) was calculated as 0.0042. It can be observed that only the diagonal value is equal to 1 while the off-diagonal values are close to zero, indicating that the noise is independent from each other among the detector bins. This result is consistent with the noise correlation analysis from repeated measurements of a different CT scanner (a GE HiSpeed four-slice CT scanner) as reported in [8].

## 4. DISCUSSIONS

The mean-variance relationship of formula (5) is theoretically based on equation (3). One assumption during the derivation of equation (3) is that the chance of detecting zero photon number is small because of the logarithm transform. Given the line integral variance $\sigma_{p_i}^2$ from repeated measurements, the mean of the transmitted photon number $N_d$ can be estimated according to equation (3). The range of the transmitted photon number varies noticeably at different bins and also at different mAs levels. Figure 10 shows the number of transmitted photons at the same projection view as in Figure 7. It can be observed that even at the 17 mAs level, the minimum number of transmitted photons is approximately 10. The probability of receiving a zero photon number for a random variable of Poisson distribution with mean value 10 is very small ($4.5\times10^{-5}$). Therefore, the assumption behind the equation (3) generally holds in all the experiments reported in this paper up to the lowest level of 17 mAs.

As shown in Figure 7, a significant quantity of sinogram data from the highly attenuating region at very low mAs level (17 mAs) failed the normality test (i.e., their p-values are less than 0.05). Strictly speaking, their PDFs cannot be expressed as a Gaussian functional. Therefore, a cost function of the Gaussian functional for noise reduction and image reconstruction at such low mAs levels may not be mathematically adequate.

Theoretically, the compound Poisson PDF would be an option to construct a cost function for statistical noise treatment and image reconstruction from the transmitted projection data in the transmission space. In the transmission space, image reconstruction from the transmitted data is a nonlinear problem because the system matrix relating the source to the data is nonlinear. It is well known that solving a nonlinear problem is much more challenging than solving a linear problem. The solution of a non-linear system is less stable than that of a linear system in the presence of noise. In addition, minimizing the compound Poisson cost function is numerically tedious and, therefore, an approximation by the Poisson distribution is usually taken.

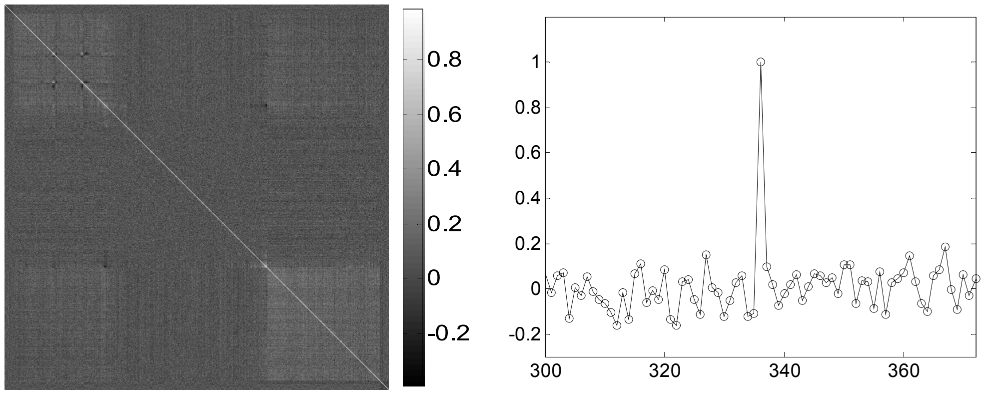


Figure 9: (left) correlation coefficients matrix of the noise among detector bins from repeated measurements of a view angle at the 17 mAs level; (right) the horizontal profiles through the center of (left). It can be observed that only the diagonal value is equal to 1 while the off-diagonal values are close to zero.

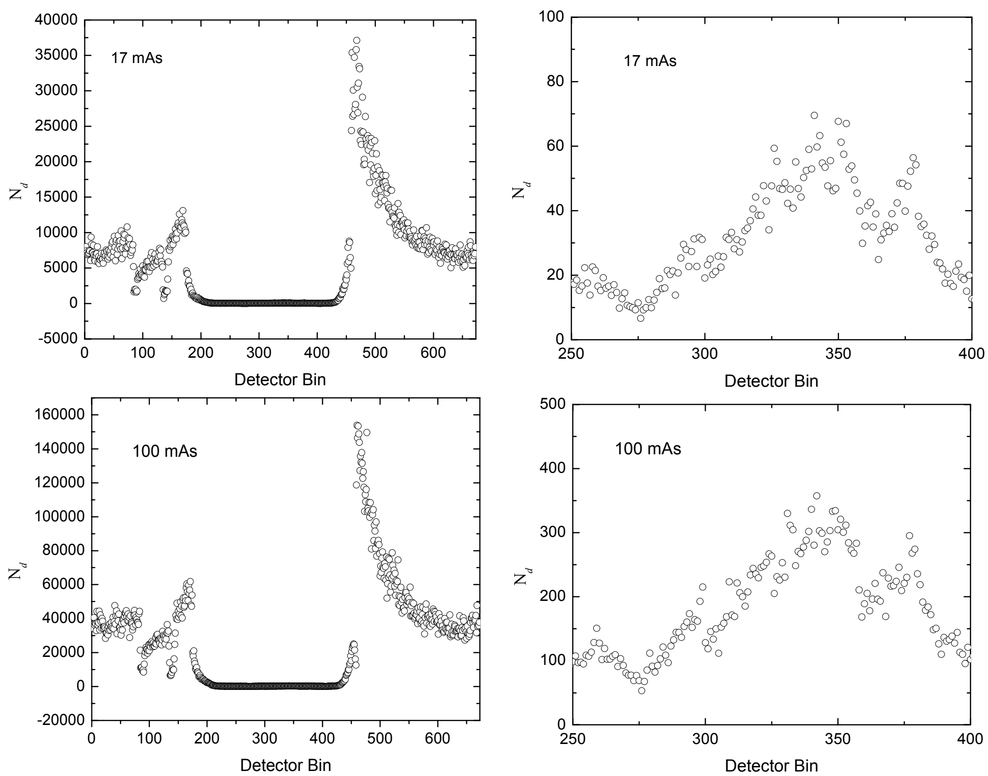


Figure 10: Number of the transmitted photons along one projection view at (top left) the 17 mAs level and (bottom left) the 100 mAs level for all detector bins; (top right) and (bottom right) show the detector bins between 250 and 400 for the 17 mAs and the 100 mAs levels respectively.

Seeking an adequate PDF for the sinogram data in Radon space, where image reconstruction from the sinogram data is a linear problem, remains an active research topic [2]. If the exact PDF is unknown but close to a normal distribution, as shown in Figure 8, a penalized weighted least-squares (PWLS) cost function can be an optimal choice, which fully utilizes the relationship between the first and second statistical moments. Our previous work utilizing this alternative approach has generated very encouraging results in terms of high computational efficiency and reconstruction accuracy as measured by noise-resolution tradeoff and receiver operating characteristic (ROC) merits [8, 9].

## 5. CONCLUSIONS

In this work, we studied the noise properties of CT sinogram data at low mAs levels through repeated experiments on an anthropomorphic torso phantom. We performed the Shapiro-Wilk normality test on the repeated measurements and found that data channels at highly attenuating regions failed the test at very low mAs levels.

Based on the repeated experiments, we validated the mean-variance relationship of each data channel at different mAs levels. The variance of projection data at a specific detector bin are completely determined by two physical quantities: (a) the line integral of attenuation coefficients along the X-ray path and (b) the incident photon number. Our noise model of equation (5) considered these two quantities elegantly. The first quantity is reflected by $\overline{p}_i / \eta$ in equation (5), where $\eta$ is a system-specific scaling parameter. The second quantity is reflected by $f_i$ in equation (5). From our systematic studies using repeated measurements, it can be observed that factor $f_i$ primarily depends on the incident photon number (or the mAs level) and the shape of the Bowtie attenuating filter across the FOV. Essentially, $f_i$ is determined by the incident photon number at each specified detector bin. Given equation (5) and the sinogram data acquired at a given mAs level, we are able to estimate the sinogram variances very accurately. It is expected that the normality test and especially the validated mean-variance relationship of equation (5) would assist the sophisticated image reconstruction methodologies in current CT scanners to address the noise problem in low-dose CT clinical applications. The statistical PWLS approach is offered as an example for low-dose CT imaging, as demonstrated by our previous research [8, 9].

## ACKNOWLEDGEMENT

This work was supported in part by the National Institutes of Health under Grant #CA082402. Dr. H. Lu was supported by the National Nature Science Foundation of China under Grant 30470490. We would like to thank Mr. Danny Gallagher of Stony Brook University Hospital and Messrs. David Bradley, Bernhard Schmidt and Hank Urban of Siemens Medical Solutions for their assistance on data acquisition. The authors are grateful to Ms. Jennifer Segui and Ms. Aimee Minton for editing this paper.

## REFERENCES

[1] Herman G T, "*Image Reconstruction from Projections*", Academic Press, New York, 1980.

[2] Li T, Li X, Wang J, Wen J, Lu H, Hsieh J, and Liang Z, "Nonlinear sinogram smoothing for low-dose X-ray CT", *IEEE Trans. Nuclear Science*, vol.51, no. 4, pp. 2505-2513, 2004.

[3] Lin L I K, "*A concordance correlation coefficients to evaluate reproducibility*". Biometrics, vol. 45, no. 3, pp. 255-268, 1989.

[4] Linton O W and Mettler F A, "National conference on dose reduction in CT, with an emphasis on pediatric patients", *American Journal of Roentgenology*, vol. 181, no. 2, pp. 321-329, 2003.

[5] Lu H, Li X, Hsiao I-T, and Liang Z, "Analytical noise treatment for low-dose CT projection data by penalized weighted least-square smoothing in the K-L domain", *SPIE Medical Imaging*, vol. 4682, pp. 146-152, 2002.

[6] Macovski A, "*Medical Imaging Systems*", Prentice-Hall Inc., New York, 1982.

[7] Snyder D L and Miller M L, "*Random point Processes in Time and Space*", Springer-Vertag, New York, 1991.

[8] Wang J, Li T, Lu H, and Liang Z, "Penalized weighted least-squares approach to sinogram noise reduction and image reconstruction for low-dose X-ray computed tomography, *IEEE Trans. Medical Imaging*, vol.25, no. 10, pp. 1272-1283, 2006.

[9] Wang J, Li T, Lu H, and Liang Z, "Noise reduction for low-dose single-slice helical CT sinograms", *IEEE Trans. Nuclear Science*, vol.53, no.3, 1230-1237, 2006.

[10] Whiting B R, Massoumzadeh P, Earl O A, O'Sullivan J A, Snyder D L, and Williamson J F, "Properties of preprocessed sinogram data in X-ray computed tomography", *Medical Physics*, vol. 33, no. 9, pp. 3290-3302, 2006.